

Mapping of Elastic Stiffness in an $\alpha+\beta$ Titanium Alloy using Atomic Force Acoustic Microscopy

Anish KUMAR*, Ute RABE, and Walter ARNOLD†

Fraunhofer Institute for Non-Destructive Testing (IZFP), Campus E 3.1, D-66123 Saarbrücken, Germany

(Received May 8, 2008; accepted May 14, 2008; published online July 18, 2008)

The present study reports for the first time the mapping of elastic stiffness of different phases in a structural metallic material with lateral resolution of less than 100 nm. The distribution of elastic stiffness across the α , β , and α' phases in Ti–6Al–4V alloy has been studied using atomic force acoustic microscopy. The experimentally obtained indentation modulus values for the various phases in the titanium alloy are compared with those estimated in literature. The effect of crystallographic orientation of phases on the indentation modulus is also discussed. [DOI: 10.1143/JJAP.47.6077]

KEYWORDS: atomic force microscopy, atomic force acoustic microscopy, indentation modulus, titanium alloy

1. Introduction

The elastic properties of multiphase structural materials are governed by those of the individual phases. These are important parameters to study the response in the deformation behavior, in crack nucleation and the crack propagation, and the measurement of stresses by X-ray diffraction in non-destructive testing and material science depends critically on the knowledge of elastic constants of the phases. Atomic force acoustic microscopy (AFAM) combines ultrasonics with atomic force microscopy (AFM) and can be used for elastic stiffness measurement with a lateral resolution of a few tens of nanometers.¹⁾ AFAM has been used extensively for measurement of elastic properties of thin films,²⁾ piezoelectric ceramic materials,³⁾ clay,⁴⁾ glass-fiber/polymer matrix composites,⁵⁾ and nano-crystalline materials.^{6,7)} However, no study is reported so far for variation in elastic stiffness across different phases in multiphase metallic materials using AFAM. Recently, there was a report on the elastic-stiffness distribution on dual-phase stainless steel obtained by resonance-ultrasound microscopy (working on a similar basic principle as that of AFAM but for larger load and tip radius) with a step size of 5 μm .⁸⁾

The physical and mechanical properties of $\alpha+\beta$ titanium alloys are highly dependent upon the type and amount of various phases formed during the heat treatments. Unlike other alloys, elastic properties of $\alpha+\beta$ titanium alloys are highly affected by the thermal/thermo-mechanical treatments.^{9,10)} Depending upon the heat treatment temperature and cooling rate, the microstructure of the titanium alloys may consist of different volume fraction of α , β , unstable β , and/or α' phases.⁹⁾ The volume fraction of β phase increases with increasing temperature up to the β transus temperature. Upon cooling to room temperature, the β phase becomes unstable and transforms to stable β and secondary α if enough time is given for the diffusion to take place. If the alloy is quenched to room temperature (diffusion is not allowed), the β phase becomes unstable and either remains as unstable β , or transforms to soft α'' or hard α' martensite, depending upon the soaking temperature, alloy chemistry and cooling

rate. The unstable β has been reported to be a soft phase having the lowest moduli and highest damping among various phases in titanium alloys.⁹⁾ Recently, Kumar *et al.*¹¹⁾ have studied the solution annealing behavior in various $\alpha+\beta$ and β titanium alloys using ultrasonic measurements. They have shown that the ultrasonic velocity and hence the elastic moduli of the $\alpha+\beta$ titanium alloys decreases with increasing solution annealing temperature at which the specimen was soaked followed by water quenching, up to an intermediate temperature, ~ 1123 K for Ti–6Al–4V. The ultrasonic velocity then increased continuously until the β transition temperature remaining constant beyond.^{11,12)} The minimum Young's modulus in the specimen quenched from 1123 K was found to be 111.5 GPa increasing to 114 and 115 GPa in the specimens quenched from 1223 and 1273 K, respectively.¹²⁾ The modulus was found to be ~ 116 GPa in the specimen quenched from 973 K.¹²⁾ The minimum elastic moduli obtained in the specimens solution annealed followed by water quenching from the intermediate temperature was attributed to the maximal amount of metastable β formed in the specimen.^{9,11,12)} The elastic modulus of the metastable β is believed to be the minimum among various phases. Fan¹³⁾ has calculated the modulus of various phases of Ti–6Al–4V from the modulus values in the specimens having different volume fraction of α , β , and α' phases. He reported that the modulus of the β phase is minimum (82 GPa) followed by α' martensite (113 GPa), and α phase (117 GPa), respectively.¹³⁾

Even though several studies have been reported for lower modulus of the β phase based on the average modulus of the specimen with α , β , and α' phases, no study has been reported so far for direct measurement of the elasticity of these individual phases. In the present study, an attempt is made for mapping the elastic stiffness distribution in a dual phase Ti–6Al–4V alloy with a lateral resolution of better than 100 nm.

2. Principle of AFAM

The experimental set-up and the principle of the AFAM technique are discussed in detail elsewhere.^{1–3,6)} The principle of AFAM in very brief and the equations used in the present study for deriving the indentation modulus of the specimen from the contact resonance frequencies are presented below. In AFAM, an ultrasonic transducer injects longitudinal waves from the bottom surface into the sample causing ultrasonic vibrations of its opposite (top) surface.

*On leave from Metallurgy and Materials Group, Indira Gandhi Centre for Atomic Research, Kalpakkam 603102, Tamil Nadu, India.
E-mail address: anish@igcar.gov.in

†Present address: Department of Materials, Campus D 2.2, Saarland University, D-66123 Saarbrücken, Germany.

These vibrations couple via the tip into the AFM cantilever and excite it to bending vibrations. Likewise, one might excite the cantilever chip with the integrated piezo-electric transducer.¹⁴⁾ This technique is often referred to as ultrasonic atomic force microscopy (UAFM). The high-frequency cantilever vibrations can be detected with the same split-photo detector as used for topography measurements. The spatial resolution is given by the tip-sample contact radius a_c , and is of the order of a few 10 nm. The resonance frequencies of the spring-coupled system shift to higher values, called contact-resonances, due to the elastic restoring forces of the sample surface acting to the tip. The higher contact-resonance frequency for a cantilever indicates higher contact stiffness and hence higher indentation modulus of the specimen, if the tip properties and the load applied are the same.¹⁾ Using a suitable mechanical model to describe the vibration of the AFM cantilever beam in contact with the sample surface, it is possible to obtain quantitative values of the normalized contact stiffness k^*/K_c , where k^* and K_c are the contact stiffness and the spring constant of the cantilever, respectively, from the shift of the contact-resonance frequencies relative to the free cantilever beam-resonances. For evaluation of the normalized contact stiffness, two resonance frequencies of the clamped-spring coupled system are required.¹⁾

For indentation modulus measurements using AFAM, a reference material with known elastic constants, usually an amorphous material or a single-crystal material with known orientation is used to derive the indentation modulus of the test sample using the following relation:

$$\frac{E_S^*}{E_R^*} = \left(\frac{k_S^*}{k_R^*} \right)^{3/2}, \quad (1)$$

where k_S^* , E_S^* , k_R^* , and E_R^* are the contact stiffness and the reduced modulus of the sample and of the reference specimen, respectively. Equation (1) holds for a spherical tip. For isotropic solids, E^* is related to the elastic properties of the sample and the tip through the following equation:

$$\frac{1}{E^*} = \frac{1 - \nu_s^2}{E_s} + \frac{1 - \nu_{tip}^2}{E_{tip}}. \quad (2)$$

Here, $E_{s,tip}$ are the Young's moduli of the sample and of the tip, respectively, and $\nu_{s,tip}$ are the corresponding Poisson ratios. In the case of anisotropic solids an indentation modulus M is introduced, which can be calculated from the single-crystal elastic constants and the corresponding orientations.¹⁵⁾ If there exists a three- or four-fold rotational symmetry axis perpendicular to the boundary, the contact area is circular. This holds for silicon sensor tips, which are oriented in the (001) direction. In this case eq. (2) can be replaced by:

$$\frac{1}{E^*} = \frac{1}{M_s} + \frac{1}{M_{tip}}, \quad (3)$$

where M_s and M_{tip} are the indentation moduli of the sample and the tip, respectively.^{3,15)} For isotropic bodies, the indentation modulus is $M = E/(1 - \nu^2)$ and eq. (3) is equivalent to eq. (2).

3. Experimental Procedure

Specimens of 8 mm length were obtained from a Ti-6Al-4V alloy rod of 10 mm diameter, supplied by Goodfellow.

Two specimens were solution treated at 1323 K for 1 h followed by water quenching. These specimens were subsequently heat treated at 1123 K for 1 h, and at 1223 K for 1 h respectively, followed again by water quenching. The surface of the specimens were polished as per the standard practice for metallography up to 1200 grit SiC paper followed by polishing with 0.25 μ m diamond paste. At least 2 mm of material was removed during the initial polishing to remove all the oxide layers and oxygen entrapment from the surface. The specimens were analyzed in the as polished condition. In specimen with different phases, preferential polishing is obtained by the use of fine-grade diamond paste ($< 1 \mu$ m).¹⁶⁾ Hence, the duration of polishing with 0.25 μ m diamond paste was optimized to get the minimum topography to resolve the phases without influencing the AFAM measurements.

A Solver P47H (NT-MDT) scanning probe microscope with a facility for acquiring the contact spectra at every point of the area under investigation was used. So-called NCL type cantilevers with an uncoated monolithic silicon tip oriented in [100] direction were used. These cantilevers were obtained from Nanoworld. As per the data sheet provided by the manufacturer, the spring constant and dimensions of the cantilevers used in the present study are as follows: Spring constant 31 N/m, thickness 6.4–6.5 μ m, width 34 μ m, and length 232 μ m. The experimentally determined first and the second free resonances of these cantilevers were found to be in range of 150.6–151.4 and 937.5–939.5 kHz, respectively.

The specimens' surface topography was first obtained in tapping mode to avoid excessive damage to the new tip. Based on the topography obtained in tapping mode, a location of sufficient flatness was identified for AFAM analysis. The tip was brought in contact with the specimen and a load of ~ 600 nN was applied. The contact resonance at a point in the matrix was obtained. The contact mode topography and qualitative AFAM images at frequency slightly higher than the contact resonance frequency were obtained. During the first few scans, the contact-resonance frequencies increased continuously due to broadening of the tip. The qualitative AFAM imaging was carried out for the same area for 4–5 times until the tip became stable and no shift in the contact-resonance frequency was observed while scanning. Following this, the spectra for first contact resonance were obtained at all points on the selected area with a step size of ~ 50 nm and a frequency resolution of 0.2 kHz. Similarly, spectra were also obtained on the same area for the second-contact resonance with a frequency resolution of ~ 0.5 kHz. After obtaining the second contact-resonance spectra, the first contact-resonance was again checked whether it remained the same. Following this, the first and the second-contact resonance spectra were obtained on a reference specimen, here a nickel single-crystal with (100) orientation. On Ni(100) specimen, 256 (16×16) spectra were obtained at ~ 125 nm step size.

Specific software were developed in LabVIEW for determining the peak frequencies for both the first and the second contact-spectra at every point of measurement and for calculating the distribution of contact stiffness and indentation modulus using an analytical model reported earlier.¹⁾ The distribution of indentation modulus in the specimen was derived from the corresponding contact stiffness values in the test specimen and the reference specimen using eqs. (1)–(3).

4. Results and Discussion

Figure 1 shows the tapping mode topography image of the Ti-6Al-4V sample solution annealed at 1323 K for 1 h and then water-quenched followed by annealing at 1123 K for 1 h and then water-quenching again. In Ti-6Al-4V specimen in such heat treatment condition, alpha phase precipitates and beta phase between alpha platelets are only expected. Hence based on their morphology, the phases are identified and shown in Fig. 1(a). The area selected for AFAM is also shown in this image. Figures 2(a) and 2(b) show the variation in the first and the second contact resonance frequencies, respectively. It can be seen that the β phase exhibits lower contact-resonance frequencies as compared to the α phase. Furthermore, the α phase orientated parallel to each other show similar contact-resonance frequencies. The distribution of the normalized contact stiffness derived from the two contact-resonance frequencies using a mechanical model¹⁾ is given in Fig. 2(c). The average first and the second contact-resonance frequencies in Ni(100) were found to be 605 and 1534 kHz, respectively. The indentation modulus for Ni(100) was calculated to be 233 GPa through measurements of ultrasonic longitudinal and shear wave velocities in Ni(100)

and Ni(111) single crystals and using the methodology described in detail elsewhere.^{6,15)} Determining the contact stiffness of the reference Ni(100) specimen and taking its indentation modulus as 233 GPa, the distribution of the indentation modulus for the titanium alloy specimen is derived using eq. (4) and is shown in Fig. 2(d). It can be seen in Fig. 2(d) that the indentation modulus for the β phase is about 110 and 120–130 GPa for the α phase with different orientations. As the single crystal elastic constants for the α phase could not be obtained from literature for similar chemical composition, the measured values of indentation modulus for α phase with different orientations are compared with that for pure Ti. The modulus reported for polycrystalline pure α -Ti (116.5 GPa)¹⁷⁾ is similar to that for α phase (117 GPa) in Ti-6Al-4V.⁹⁾ Furthermore, the chemical composition and hence the modulus of the α phase in Ti-6Al-4V alloy is reported to be similar irrespective of the temperature of treatment.⁹⁾ Hence, the indentation modulus in the α phase with different crystallographic orientations should also be in a similar range as those for pure Ti. The values of indentation modulus, calculated from the single-crystal elastic constants taken from ref. 17, for different planes of pure α -Ti are 121.1, 142.7, 121.1, 130.3, and 126.9 GPa in (100), (001), (110), (101), and (111) planes, respectively. These values match quite well with the values of 120–130 GPa obtained for the α -phase indentation moduli for different orientations as observed in Fig. 2(d).

The distribution of the first contact-resonance in another β grain in the same specimen is shown in Fig. 3(a). As the cantilever used for different measurements were different, however of the same type with slightly different tip radii, the absolute values of the resonance frequencies cannot be compared across the images. However, the range of frequency in the images of distribution of contact resonance frequencies can provide an idea about the difference in elastic stiffness of various phases present in the image. Further, as the difference in the specifications of all the cantilevers used

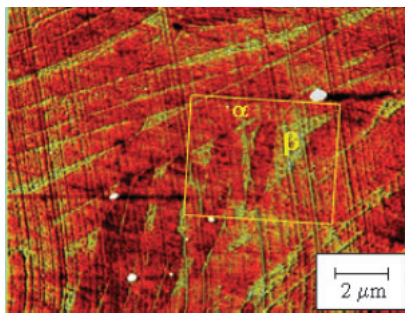


Fig. 1. Tapping mode topographic image of the Ti-6Al-4V sample showing the area selected for the AFAM measurements (z -scale = 4 nm).

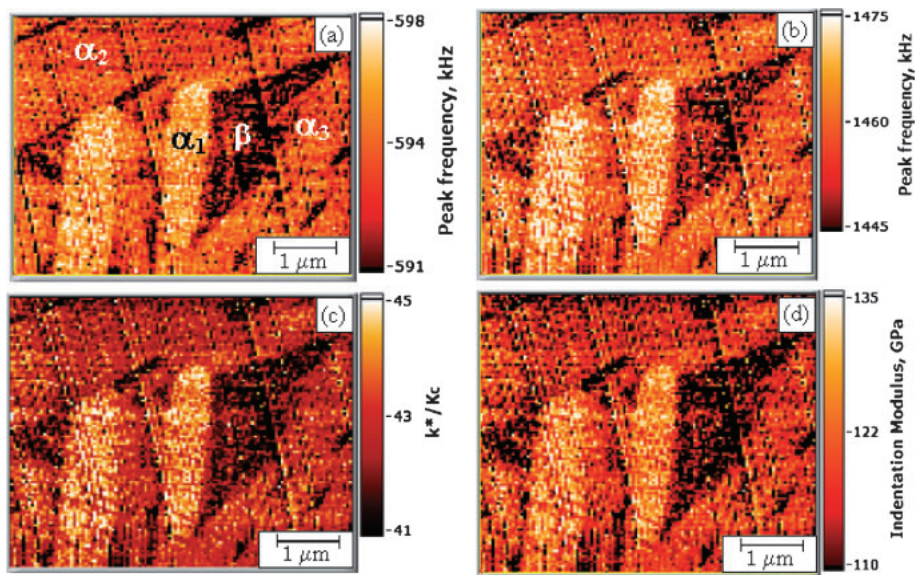


Fig. 2. (a) Distribution of first contact-resonance frequency, (b) second contact-resonance frequency, (c) k^*/K_c , and (d) indentation modulus of the Ti-6Al-4V specimen heat treated at 1123 K for 1 h followed by water quenching. The three different variants of alpha phase are marked in (a) as α_1 , α_2 , and α_3 in decreasing order of their indentation modulus as observed experimentally.

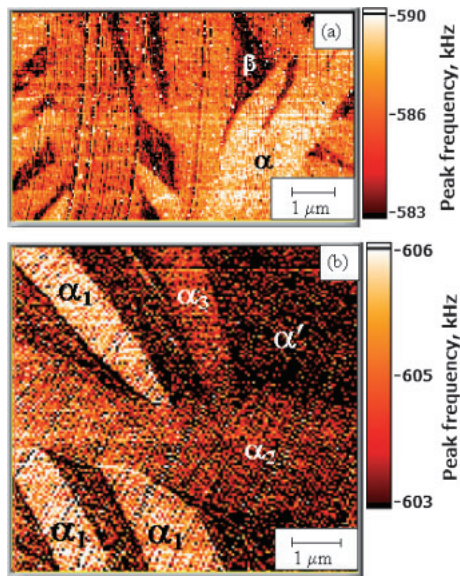


Fig. 3. Distribution of the first contact-resonance frequency in the Ti-6Al-4V specimens heat treated at (a) 1123 and (b) 1223 K for 1 h followed by water quenching. The three different variants of alpha phase are marked in (b) as α_1 , α_2 , and α_3 in decreasing order of their indentation modulus as observed experimentally.

in the present study is insignificant, the range of frequencies in different images can also be compared. It can be seen from Figs. 2(a) and 3(a) that the range of contact-resonance frequencies is almost similar (~ 7 kHz) for the specimen quenched from 1123 K in different grains, demonstrating the reliability of the technique. Figure 3(b) shows the variation in the first contact-resonance frequency for the specimen quenched from 1223 K. A maximum difference of ~ 3 kHz is obtained in this specimen [Fig. 3(b)] as compared to ~ 7 kHz for the specimen quenched from 1123 K [Figs. 2(a) and 3(a)]. This is attributed to the fact that with an increase in the heat treatment temperature, the volume fraction of the β phase increases at the heat treatment temperature. This β phase has a lower amount of β stabilizing element and it transform to α' martensite upon fast cooling through water quenching.^{9,11} Hence, the specimen heat treated at 1223 K followed by water quenching consists of primary α and α' martensite, unlike the specimen heat treated at 1123 K followed by water quenching which consists of primary α and metastable β phase. It can be seen in Fig. 3(b) that the contact-resonance frequency for α' martensite matrix is marginally lower than that for the α phases with orientation showing minimum contact-resonance frequency (α_2 and α_3). This indicates that the indentation modulus of the α' martensite is marginally lower than that for the α phase. The present study confirms through the direct measurement on individual phases that the metastable β phase has the minimum modulus followed by α' and α phases in Ti-6Al-4V alloy. These results are in good agreement with the estimate of Fan¹³ for individual phases and with the report of Kumar¹² for the average Young's modulus of the specimens containing these phases.

It can be seen that the range of the indentation modulus for α phase in planes with the extreme values is only about 20 GPa. This indicates that the AFAM measurements can unambiguously differentiate two phases in titanium alloys

irrespective of their orientation, if the difference in the indentation modulus is more than ~ 20 GPa, as for α and β phases in the present case. This also demonstrates the applicability of AFAM for microstructural characterization applications with a lateral resolution of better than 100 nm, based on the difference in the elastic properties of various phases.

5. Conclusions

The present study reports the mapping of elastic stiffness of different phases in a structural metallic material with lateral resolution of less than 100 nm. The indentation modulus values for various phases in the $\alpha+\beta$ titanium alloy Ti-6Al-4V as measured by AFAM is found to be in very good agreement with those predicted in literature. The results also indicate that the effect of crystallographic orientation of α phase on the indentation modulus can also be characterized using AFAM. The study also demonstrates the applicability of AFAM for microstructural characterization applications with a lateral resolution of better than 100 nm, based on the difference in the elastic properties of various phases present.

Acknowledgements

One of the authors (A.K.) would like to thank the Alexander von Humboldt Foundation, Bonn, Germany, for providing financial support with a post-doctoral fellowship. He is also thankful to Dr. Baldev Raj, Director, Indira Gandhi Centre for Atomic Research, Kalpakkam, for continuous encouragement and support. We are thankful to Dr. S. Hirsekorn, Fraunhofer Institute for Non-Destructive Testing, Saarbrücken, for many useful discussions. The invited talk given by one of the authors (W.A.) at the ICSPM15 in Atagawa in December 2007 contained part of this paper.

- 1) U. Rabe: in *Applied Scanning Probe Methods II*, ed. B. Bhushan and H. Fuchs (Springer, Heidelberg, 2006) p. 37.
- 2) U. Rabe, S. Amelio, E. Kester, V. Scherer, S. Hirsekorn, and W. Arnold: *Ultrasonics* **38** (2000) 430.
- 3) U. Rabe, M. Kopycinska, S. Hirsekorn, J. M. Saldana, G. A. Schneider, and W. Arnold: *J. Phys. D* **35** (2002) 2621.
- 4) M. Prasad, M. Kopycinska, U. Rabe, and W. Arnold: *Geophys. Res. Lett.* **29** (2002) 1172.
- 5) A. B. Kos and D. C. Hurley: *Meas. Sci. Technol.* **19** (2008) 015504.
- 6) M. Kopycinska-Müller, A. Caron, S. Hirsekorn, U. Rabe, H. Natter, R. Hempelmann, R. Birringer, and W. Arnold: *Z. Phys. Chem.* **222** (2008) 471.
- 7) M. Kopycinska-Müller, R. H. Geiss, J. Müller, and D. C. Hurley: *Nanotechnology* **16** (2005) 703.
- 8) H. Ogi, H. Niho, and M. Hirao: *Acta Mater.* **54** (2006) 4143.
- 9) Y. T. Lee and G. Welsch: *Mater. Sci. Eng. A* **128** (1990) 77.
- 10) G. J. Gil, J. M. Manero, and J. A. Planell: in *Proc. 8th World Conf. Titanium '95: Science and Technology*, ed. P. A. Blenkinsop, W. J. Evans, and H. N. Flower (Maney Publishing, London, 1995) p. 2454.
- 11) A. Kumar, T. Jayakumar, B. Raj, and D. Banerjee: *Philos. Mag.* **88** (2008) 327.
- 12) A. Kumar: Ph. D. Thesis, Indian Institute of Technology, Kharagpur, India (2005).
- 13) Z. Fan: *Scr. Metall. Mater.* **29** (1993) 1427.
- 14) K. Yamanaka, A. Noguchi, T. Tsuji, T. Koike, and T. Goto: *Surf. Interface Anal.* **27** (1999) 600.
- 15) J. J. Vlassak and W. D. Nix: *Philos. Mag. A* **67** (1993) 1045.
- 16) J. B. J. W. Hegemana, J. Th. M. De Hosson, and G. de With: *Wear* **248** (2001) 187.
- 17) G. Simmons and H. Wang: *Single Crystal Elastic Constants and Calculated Aggregate Properties: A Handbook* (MIT Press, Cambridge, MA, 1971) 2nd ed.